Cellulose nanocrystal surface functionalization for the controlled sorption of water and organic vapours

Etzael Espino-Perez, Julien Bras, Giana Almeida, Perla Relkin, Naceur Mohamed Belgacem, Cedric Plessis, Sandra Domenek

Cellulose nanocrystal surface functionalization for the controlled sorption of water and organic vapours

Etzael Espino-Pérez · Julien Bras · Giana Almeida · Perla Relkin · Naceur Belgacem · Cédric Plessis · Sandra Domenek

Abstract The surface grafting of cellulose nanocrystals (CNC) is a valuable tool to increase opportunities for their application. This work had several goals designed to improve CNC: reduction of hornification, increased re-dispersibility after CNC drying, and tuning of the surface graft to enhance the adsorption of particular molecules. To achieve this, the CNC surfaces were modified chemically with aromatic surface grafts using widely employed methods: the creation of urethane linkages, silylation and esterification. Even a low degree of grafting sufficed to increase water contact angles to as much as 96°. The analysis of water sorption isotherms showed that at high water activities, capillary condensation could be suppressed and hysteresis was decreased. This indicates that hornification was significantly suppressed. However, although the contact angles increased, the water sorption isotherms were changed only slightly because of reduced hysteresis. The grafts were not able to shield the surface from water vapour sorption. A comparison of the sorption isotherms of anisole and cyclohexane, sorbates with a similar surface area, showed that the sorption of anisole was three times higher than that of cyclohexane. The specific sorption of aromatic molecules was achieved and the most efficient methodology was the esterification of CNC with carboxylic acids containing a flexible linker between the aromatic moiety and ester bond.

Keywords Cellulose nanowhiskers · Chemical surface modification · Water sorption · Organic vapour sorption · GAB model

E. Espino-Pérez · G. Almeida · P. Relkin · C. Plessis · S. Domenek (✉)
UMR Ingénierie Procédés Aliments, AgroParisTech, INRA, Université Paris-Saclay, 91300 Massy, France
e-mail: sandra.domenek@agroparistech.fr

E. Espino-Pérez · J. Bras · N. Belgacem
Université Grenoble Alpes, LGP2, F-38000 Grenoble, France

E. Espino-Pérez · J. Bras · N. Belgacem
CNRS, LGP2, F-38000 Grenoble, France

Introduction

Cellulose nanocrystals (CNC) obtained by the acid hydrolysis of microcrystalline cellulose (MCC) can be used in a broad range of applications; in addition to their functional properties, they also have the benefits of being biobased, non-toxic and biodegradable (Mariano et al. 2014; Rodrigues et al. 2014; Wu and Zhang 2014). The advantages of the non-porous structure, large surface area, low density, high aspect ratio and high tensile strength of CNC have been already exploited in different domains, such as controlled drug delivery systems, the encapsulation and delivery of molecules of technological interest (essential oils,

fertilizers, etc.), the depollution of aqueous environments (Lam et al. 2012), water treatment (Carpenter et al. 2015), and the development of bionanocomposites (Habibi 2014; Mariano et al. 2014).

The abundance of hydroxyl groups on the CNC surface generates surface reactivity that can be utilized to tailor surface properties (Habibi et al. 2010). There are several examples of their use to develop absorbents for water depollution. Alila et al. (2011) grafted stearic acid by esterification on starch nanocrystals in order to remove aromatic compounds from water. These nanocrystals displayed a high affinity for xylene and quinoline. The modification of oxidized CNC surfaces with C16 surfactants produced the co-adsorption of 2-naphthol (Alila et al. 2005). The grafting of cellulose fibres with different amino derivatives resulted in an improvement of up to 800 % in the adsorptive capacity of aromatic organic compounds (Alila and Boufi 2009), and grafting polystyrene onto CNC enhanced the adsorption of 1,2,4-trichlorobenzene from water by 20 % (Morandi et al. 2009). An interesting study was published by Korhonen et al. (2011) who developed a hydrophobic, floating nanocellulose aerogel for the purification of water by oil adsorption. With respect to the development of bionanocomposites, CNC surface grafting is of great importance to ensuring the compatibility of CNC with hydrophobic polymer matrices (Mariano et al. 2014) and the re-dispersibility of dried CNC powders. Primary CNC, like MCC, suffer irreversible aggregation due to strong hydrogen bonding between the particles once they are dried (Eyley and Thielemans 2014). For example, hornification following the drying of MCC is a major problem encountered in the formulation of pharmaceutical excipients (Kachrimanis et al. 2006). Surface grafting to reduce inter-particle hydrogen bonding is one of the solutions to this problem (Habibi et al. 2010). Moreover, the advantage of using surface grafted CNC to improve the mechanical and barrier properties of bionanocomposites has been demonstrated by a number of authors (Ambrosio-Martin et al. 2015; Espino-Perez et al. 2013, 2016a; Follain et al. 2013; Fortunati et al. 2013). The reason suggested for the enhanced barrier properties of the materials was an improved distribution of the nanocrystals inside the polymer, allowing for higher tortuosity effects.

Based on these results, the rationale for the present work was to develop grafted CNC surfaces that could fulfil the functions of an absorbent of a specific class of volatile molecules, facilitate the re-dispersibility of dried powders and enhance the compatibility of CNC with polymer matrices. For this purpose, aromatic surface grafts were chosen in order to permit electrostatic π–π interactions with volatile molecules bearing aromatic functions.

The hydrophobic behaviour of an aromatic surface graft might possibly be used to enhance compatibility with polymer matrices. For example, the widely employed biobased polymer polylactide displays strong affinity for aromatic molecules (Salazar et al. 2014). Working with molecules bearing aromatic moieties is also relevant to their applications, as they are largely present in undesirable environmental pollutants or, on the contrary, can be used positively in the food and fragrance industries. In both cases, it would be useful to be able to reversibly sorb volatile molecules in/on solid substrates. In the first case, this would enable the creation of reversible absorbents for the decontamination of polluted environments, while in the second case, controlled release systems could be developed (Lemahieu et al. 2011). The use of materials with strong barrier properties against aromatic volatile compounds for packaging systems is also an effective means of protecting the quality of packaged goods. Indeed, it has been suggested that reversible absorbents distributed inside polymer materials might be a way to obtain strong barrier properties (Clemenson et al. 2010; Fang et al. 2012; Hanson et al. 2012).

The approach adopted for this work was to study the impact of the CNC grafting method and the chemical structure of the surface graft on the physisorption of water and volatile organic molecules. To achieve this, CNC were grafted using three widely employed routes for surface grafting, namely the formation of a urethane linkage, esterification and silylation. The physical and chemical characteristics of the different powders were analysed. To determine the absorbent capacity of the grafted CNC powders, the sorption isotherms of water, anisole and cyclohexane were recorded. Water sorption isotherms could provide information on the moisture sensitivity of CNC samples, while anisole (4-methoxy benzene) and cyclohexane are volatile organic compounds with a similar surface area, anisole being a non-toxic aromatic compound. By comparing the sorption isotherms of anisole and cyclohexane, it would be possible to conclude as to the specific sorption of aromatic molecules in aromatic surface grafts.

Experimental section

Materials

Microcrystalline cellulose (MCC) AVICEL® PH-101 was acquired from Sigma-Aldrich (France) and used as the raw reference material for the production of cellulose nanocrystals (CNC). Octadecyl isocyanate (ICN.Od), phenyl isocyanate (ICN.Ph), phenyl butyl isocyanate (ICN.PhBut), phenylacetic acid (PhAA), hydrocinnamic acid (BzAA), trimethoxy(phenyl)silane (TMPS), dibutyltin dilaurate, anisole and cyclohexane were obtained from Aldrich (France). Sulphuric acid (>95wt), chloroform, acetone and ethanol were purchased from Chimie-Plus.

Production of cellulose nanocrystals

Cellulose nanocrystals were prepared by the acid hydrolysis of bleached microcrystalline cellulose, adapting the optimized protocol described by Bondeson et al. (2006). MCC at a concentration of 7.1 wt% was dispersed in water. Sulphuric acid was added slowly to reach a concentration of 64 wt%. The acid hydrolysis of MCC was carried out at 44 °C for 130 min under mechanical stirring. The excess of sulphuric acid was removed by the application of water exchange/centrifugation cycles and the suspension was dialysed in deionized water for 1 week. The system was homogenized using an Ultra-Turrax T25 homogenizer (France) and subjected to an ultrasound source (Branson 250 sonifier). Finally, the CNC suspension was neutralized and a drop of chloroform was added in order to prevent microbial development.

Chemical modification of cellulose nanocrystals

Figure 1 shows the chemical structure of the functionalised CNC. The following grafting methods were used:

Carboxylic acids (phenylacetic acid, hydrocinnamic acid)

The esterification of CNC with carboxylic acids was achieved using the recently described SolReact method (Espino-Perez et al. 2014). A CNC suspension (10 wt%, pH 4.3) was subjected to ultrasound treatment for 3 min. The CNC suspension was then placed in an oil bath at 130 °C inside a balloon flask mounted with a closed distillation system. After 10 min., ten equivalents (according to the CNC dry weight) of carboxylic acid were added and the reaction mixture was agitated for 20 h under continuous water removal by distillation. The reaction work up consisted in removing unreacted carboxylic acids by dispersion–centrifugation cycles with ethanol. In the remainder of this paper, CNC grafted with phenylacetic acid is abbreviated as CNC-g-PhAA and that grafted with hydroxycinnamic acid as CNC-g-BzAA.

Alkoxysilane (trimethyl(phenyl)silane)

A variant of the SolReact method was used for the silylation of CNC with trimethyl(phenyl)silane (TMPS) (Espino-Perez et al. 2016b). CNC (1.6 wt%) were dispersed in the ethanol/water/acetic acid solvent mixture (80/16/4 wt%). The suspension was subjected twice to ultrasound treatment for 2 min. Ten equivalents of TMPS (according to the CNC dry weight) were added and the TMPS was left to hydrolyse and absorb to the CNC surface for 2 h at 25 °C under mechanical stirring. The pH was then adjusted to 7 with NaOH. The CNC/TMPS suspension was decanted into a balloon flask mounted with a distillation system and placed in an oil bath at 120 °C. After the total evaporation of ethanol and water, the reaction was continued for 3 h. Ungrafted and condensed TMPS was removed by dispersion–centrifugation cycles with water, ethanol and acetone. Finally, the CNC-g-TMPS suspension in acetone was subjected to ultrasound treatment before storage.

Isocyanates (octadecyl, phenyl and phenyl butyl)

CNC were grafted according to a protocol adapted from (Siqueira et al. 2010). CNC were suspended in dry toluene after the acetone/chloroform/toluene solvent exchange sequence. Ten equivalents of isocyanate were added according to the hydroxyl groups available at the surface of the cellulose nanoparticles ($\sim$10 wt%). The reaction was carried out under nitrogen atmosphere at 110 °C using dibutyltin dilaurate as the catalyst. The reaction mixture work up consisted in centrifugation/dispersion cycles to remove amines and unreacted isocyanates. Finally, the suspensions of CNC grafted with octadecyl isocyanate (CNC-g-ICN.Od), phenyl isocyanate

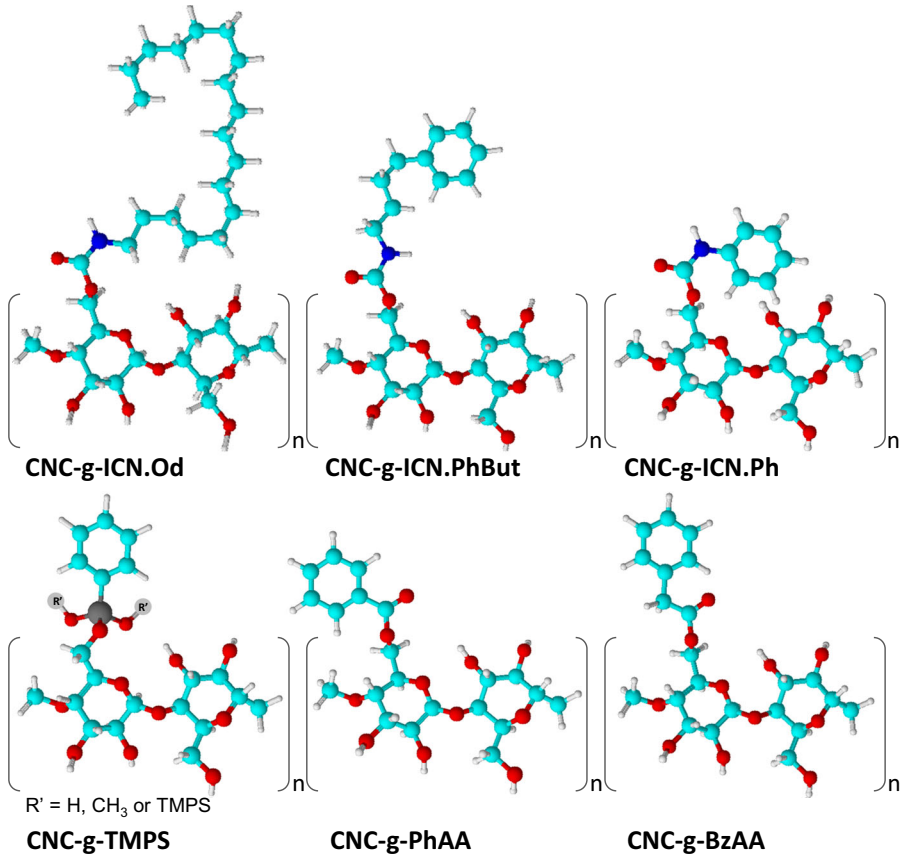

Fig. 1 Chemical structure of CNC grafted with octadecyl isocyanate (CNC-g-ICN.Od), phenyl isocyanate (CNC-g-ICN.Ph), phenyl butyl isocyanate (CNC-g-ICN.PhBut), trimethyl(phenyl)silane (CNC-g-TMPS), phenylacetic acid (CNC-g-PhAA) and hydroxycinnamic acid (CNC-g-BzAA). Atom colour nomenclature: *red* oxygen, *light blue* carbon, *light grey* hydrogen, *dark blue* nitrogen, *dark grey* silicon. (Color figure online)

(CNC-g-ICN.Ph) and phenyl isocyanate (CNC-g-ICN.PhBut) were stored in chloroform.

Environmental scanning electron microscopy (ESEM)

Environmental electron microscopy at different RH of CNC and CNC-g-BzAA was carried out using a FEI Quanta 200 microscope at 7 Torr, 8.5 kV, spot size 4.5, and with a Gaseous Secondary Electron Detector (GSED). The samples were dispersed on carbon tape. The initial conditions were set at 20 °C and 40 % RH. The samples were equilibrated for at least 10 min. The temperature was then lowered to 9 °C at the same water vapour pressure in order to create an atmosphere at 80 % RH. The samples were equilibrated for 10 min and images were captured regularly during this time.

Characterisation of cellulose nanocrystals

Sample preparation

Preparation of the powders for analysis consisted in drying CNC suspensions at room temperature for 24 h. The CNC powders were ground manually for 15 min with the using a porcelain mortar and stored at 25 °C in a desiccator over P_2O_5.

Scanning electron microscopy (SEM)

CNC were characterized by field emission scanning electron microscopy (FE-SEM), using the FEI Quanta 200 model with an accelerating voltage of 12.5 kV. The samples were fixed on a substrate with carbon tape and coated with a thin gold layer. Digital image

analysis (ImageJ Software) was used to measure the dimensions of the nanoparticles, with an average of at least 50 measurements being carried out.

X-ray diffraction (XRD)

X-ray analyses were performed using a Panalytical X'Pert Pro MPD-Ray diffractometer equipped with an X'celerator detector and operated with Ni-filtered Cu, Kα radiation ($\lambda = 1.54$ Å) generated at a voltage of 45 kV and current of 40 mA, with scanning from 5° to 60°. The CNC crystallinity index was evaluated using the Buschle-Diller and Zeronian equation, as follows:

$$I_c = 1 - \frac{I_1}{I_2} \quad (1)$$

where I_1 is the intensity at the minimum ($2\theta = 18.8°$) and I_2 is the intensity associated with the crystalline region of cellulose ($2\theta = 22.7°$). All analyses were performed at least twice.

Elemental analysis

Elemental analysis was carried out by the CNRS (National Centre for Scientific Research) Central Analytical Laboratory (Vernaison, France). Carbon, oxygen and silicon contents were measured for unmodified and modified CNC. The precision of these measurements is usually higher than the standard deviation and is commonly taken to be a maximum of ±0.2 %.

Contact angle measurements

The dynamic behaviour of the contact angle for a drop of deionised water (purified by a Micropore system) on the surface of a film of unmodified CNC, and on pressed pastilles of modified CNC, was measured for one minute before absorption of the water into the sample. A DataPhysics contact angle instrument equipped with a CCD camera was used and enabled determination of the contact angle at equilibrium, with a precision of ±1°. The kinetic of its evolution was followed for a few tens of milliseconds after deposition of the drop by capturing up to 1000 images per second. Each reported value is the average of at least triplicate measurements.

Surface area and porosity

The specific surface area of the powders was obtained from a BET analysis of N_2 adsorption isotherms using a Sorptomatic system (Thermo Electron Corporation). The specific surface area of powders was estimated by applying the Brunauer-Emmet-Teller (BET) equation within the $0.05 \leq P/P_0 \leq 0.30$ intervals of relative pressure and using a value of 16.2 $Å^2$ for the cross-sectional area of molecular N_2. A non-linear regression using the least-squares method was performed to fit the interval data in the experimental isotherms (Sorptomatic Advanced Data Processing).

Differential scanning calorimetry

Micro-DSC III (Setaram, Caluire-France) was used to measure the heat of immersion of the CNC powders in water, anisole and cyclohexane at 25 °C. A two-compartment Setaram batch mixing cell was used, where the solvent can be loaded into the upper compartment and the powder into the lower one. A bar mounted with a mixing element separates the two compartments. Manual turning of the bar opens the upper compartment and floats the powder with the solvent while mixing both. A quantity of 125 ± 2 mg of the solvent was placed in the upper compartment of the reference cell and sample cell using a micro syringe, and 10 ± 0.5 mg of CNC were placed in the lower compartment of the sample cell. Both cells were placed in the μ-DSC to await stabilization of the heat flow. The opening and mixing operation was first performed in the reference cell (50 spins for 25 s); after stabilisation of the baseline the same mixing operation was carried out in the sample cell. The heat flow signal recorded for the reference cell was subtracted from that recorded for the sample cell. Each measurement was repeated at least four times.

Aroma and water vapour sorption on cellulose nanocrystal powders

Water vapour sorption

Water sorption on unmodified and modified CNC was performed using a Dynamic Vapour Sorption (DVS) apparatus (Surface Measurement Systems Ltd.,

London, UK). MCC samples were also analysed. For each run, about 10 mg of CNC powder previously conditioned in a desiccator over P_2O_5 were analysed. Sorption isotherms and hysteresis loops were recorded at 25 °C during gradual increases/decreases in relative humidity (RH) from 0 to 90 %. Mass equilibrium was determined from the percentage change in mass with respect to time (dm/dt < 0.002 mg/min.). The water sorption values for each sample were the average of at least two measurements. Experimental error was estimated at ±5 %. Hysteresis was calculated as the mass difference between sorption and desorption mass uptake at a given activity.

Anisole and cyclohexane adsorption

The adsorption isotherms of anisole and cyclohexane were measured at 40 °C and 0 % RH using an electronic microbalance (Intelligent Gravimetric Analyser 002, Hiden Isochema Ltd, Warrington, UK) with a sensitivity of 0.2 µg. Powder samples (approximately 6 mg) were suspended in a stainless steel capsule. The microbalance itself was maintained at 50 °C to ensure stability during the weight measurements and prevent solvent condensation. Before recording the isotherms, the samples were purged in the microbalance for 24 h at 10^{-5} mbar (10^{-3} Pa) to remove all volatile compounds sorbed on the powders or present in the chamber. Aroma activity (activity = p/p_{sat}) was determined by controlling the partial pressure (p) of anisole or cyclohexane in the measurement chamber using a pressure transducer (Baratron®, MKS Instruments, Wilmington, MA, USA) linked to a tank with a vapour phase saturated in anisole or cyclohexane (p_{sat}(anisole) = 11.48804 mbar, p_{sat}(cyclohexane) = 247.76 mbar). Adsorption equilibrium was determined with dm/dt < 1 % or after 5 h of measurement. To estimate the uncertainty of measurements, analyses of anisole sorption to CNC-BzAA were carried out in triplicate and the standard deviation was calculated as being 16 %. The measurement of anisole and cyclohexane sorption in other samples was performed in duplicate and variance was within the 15 % range. Because of the long measurement times and the number of samples, the measurement campaign lasted for one year; it is therefore likely that an ageing effect of the samples might explain the broad dispersion of the values measured.

Analysis of water vapour and anisole sorption isotherms using the GAB model

A number of models have been used to describe the sorption isotherms of cellulose (one example can be found in the article by Kachrimanis et al. 2006). The models most widely used are the Brunauer-Emmett-Teller (BET) isotherm, the Guggenheim, Anderson and De Boer (GAB) isotherm, the Young and Nielson model, Parallel Exponential Kinetics (PEK), the Park model or New Dual-Mode Sorption. Preliminary analysis of the curves showed that in the present case the GAB model was most appropriate to describe our experimental data. GAB was therefore fitted to the sorption branch between 0.05 and 0.6 of water activity, using non-linear regression.

The GAB model derives from the physical adsorption theories advanced by Langmuir and Brunauer-Emmett-Teller (BET), and was derived and modified between 1946 and 1966 by Guggenheim, Anderson and De Boer (Van Den Berg 1984). This model has mainly been used to analyse food materials, pharmaceutical powders and biopolymer films, because of its broader range of applications when compared to the BET-Eq. ($0.05 < a_w < 0.8$) (Agrawal et al. 2004; Andrade et al. 2011; Follain et al. 2013; Volkova et al. 2012). It assumes localized physical multilayer sorption with no lateral interactions. The first layer of sorbed molecules covers the surface unevenly and is tightly bound in a monolayer. Subsequent layers display increasingly bulk-like properties. To account for changing properties in the outer sorbate layers, a constant K was introduced into the original BET equation, to yield the GAB equation:

$$\frac{X}{X_m} = \frac{C \cdot K \cdot a_s}{(1 - K \cdot a_s) \cdot (1 + (C - 1) \cdot K \cdot a_s)}, \qquad (2)$$

where a_s is the sorbate activity, X the grams of sorbate per gram of solid, and X_m is the monolayer capacity. The constant C is almost enthalpic in nature and accounts for the strength of sorbate binding to the primary binding sites. C is higher than unity as the sorbate in the monolayer is more stable than in the bulk (Timmermann 2003). K contains an important entropic part and corrects the properties of the multilayers with respect to the bulk liquid, thus defining the upswing of the sorption isotherm in the higher activity range. However, this should not be confused with the properties in the third sorption stage at $a_s > 0.85$. Its

value is typically smaller than unity, because molecules in the upper GAB layers have higher standard chemical potential than the liquid. K increases with stronger interactions between sorbate and sorbent (Timmermann 2003). When it approaches unity, there is almost no distinction between GAB layers and the liquid. In that case, the outer GAB layers are less structured in multilayers and more similar to the characteristics of the bulk liquid (Quirijns et al. 2005).

The specific surface areas (S) of the different samples were calculated from the monolayer values using the equation described by (Portugal et al. 2010):

$$S = X_m \frac{N_A \cdot A_m}{M}, \tag{3}$$

where N_A is Avogadro's number, A_m the cross-section of the sorbate ($H_2O = 0.125$ nm^2, anisole $= 1.36$ nm^2, cyclohexane 1.25 nm^2), and M the molar mass.

Results and discussion

Physicochemical characterisation of functionalised CNC

Table 1 shows the characteristics of the MCC and unmodified and modified CNC. The geometry of CNC did not change significantly from before to after grafting, except for CNC-g-TMPS. The degree of sample crystallinity was determined from X-Ray diffractograms using the peak height method (Park et al. 2010; Sèbe et al. 2012), taking account of the signals located at 15.7° and 22.5° which are characteristic of cellulose I. Unmodified CNC has a higher crystallinity index than MCC because of removal of the amorphous fraction. After surface grafting with ICN.Ph and ICN.PhBut, the crystallinity index fell markedly due to peeling or swelling of the surface layers because of the use of toluene at a high temperature as the reaction solvent. Surface swelling was also observed in the case of TMPS grafting. The TMPS grafting procedure yielded condensation of the siloxane structures at the CNC surface (Espino-Perez et al. 2016b), which was observed macroscopically from the formation of aggregates in chloroform. SEM analysis of the larger CNC dimensions supported this hypothesis (Table 1). Chemical modification with carboxylic acid appeared to be the best way to maintain a high crystallinity index for CNC.

The degree of substitution (shown in Table 1) was calculated from elementary analysis according to:

$$DS = \frac{C_{AGU} - X_c \cdot AGU}{X_c \cdot graft - C_{graft}} \tag{4}$$

where X_C is the fraction content of carbon in the sample, C_{AGU} and AGU are the carbon mass and total mass of an anhydroglucose unit, and C_{graft} and $graft$ are the carbon mass and total mass of the grafted molecule, respectively. The grafting of TMPS yields a high degree of substitution, which is linked to condensation of the siloxane moieties at the surface (Espino-Perez et al. 2016b).

The analysis of liquid/solid interactions showed that although the DS was low, the water contact angle was greatly increased. Some differences were observed, depending on the surface graft used. In the case of CNC-g-ICN.Od, the contact angle was high even if the DS was equal to or lower than that of the aromatic molecules. The long isocyanate chain apparently gave rise to a more hydrophobic contact angle, which was almost equal to that of CNC-g-TMPS, having a shell with a three-dimensional siloxane network (Espino-Perez et al. 2016b).

The specific surface area values (Table 1) obtained for nitrogen sorption using the BET analysis showed that CNC had a higher surface area when compared to the literature values of MCC. The order of magnitude of the specific surface area was consistent with literature values. Lu and Hsieh (2010) measured 13.362 ± 0.034 m^2/g for CNC obtained from filter paper and 27.625 m^2/g for CNC obtained from rice straw (Lu and Hsieh 2012). The measured specific surface area was much lower than the one expected from geometrical measurements CNC. For example, Dufresne (2003) announced a geometrical specific surface area of 170 m^2/g for CNC from tunicate. This difference might be explained by the aggregation of CNC in the powders through hydrogen bonding. The surface grafting can reduce aggregation, which might be the reason of the larger specific surface areas of the chemically modified CNC (Table 1).

Liquid/solid interactions between water or organic solvents and nanocellulose

The energy properties of the immersion of water, anisole and cyclohexane in grafted CNC were

Table 1 Physicaochemical characteristics of MCC, CNC and grafted CNC

Sample	Length, diameter	χ (%)	DS	Contact angle (°)	S N_2 (m^2 g^{-1})
MCC	135, 46 mm	74	0	ND	1.8[a], 1.0[b]
CNC	155, 17 nm	84[c]	0	57	22
CNC-g-ICN.Od	176, 9 nm	73	3	95	84
CNC-g-ICN.Ph	ND	65	3	96	64
CNC-g-ICN.PhBut	ND	69	2	83	78
CNC-g-TMPS	367, 62 nm	61[d]	7[d]	94	32
CNC-g-PhAA	131, 10 nm	77[c]	5[c]	75	52
CNC-g-BzAA	145, 13 nm	76[c]	3[c]	73	126

DS degree of substitution of 10 AGU moieties, χ crystallinity index, *S(N_2)* specific surface area from the N_2 isotherm

[a] Published by Portugal et al. (2010)

[b] Published by Kocherbitov et al. (2008)

[c] Published by Espino-Perez et al. (2014)

[d] Communicated by Espino-Perez et al. (2016b) using the same methodology

determined by differential scanning microcalorimetry. The enthalpy obtained by the present procedure (referred to below as the enthalpy of immersion) took account of the successive steps of (ad)sorption, wetting, and (in the case of cellulose) probably swelling of the amorphous phase as well (Douillard and Malandrini 1999). The enthalpies of immersion thus measured are presented in Table 2, which shows that the order of magnitude of enthalpy was close to what might have been expected for wetting enthalpy, because the samples were not outgassed before measurement which most probably left residual water on the CNC surface. For example, the wetting enthalpy of MCC (Avicel) by water was measured at −3.7 J/g (Douillard and Malandrini 1999), while the immersion enthalpy of Avicel (of approximately −3 J/g) was measured using a comparable method by Roskar and Kmetec (2005). The exothermic immersion enthalpy of CNC in water can easily be explained by the high contact angles and hence the high surface energy of CNC, because of polar interactions and hydrogen bonding. The immersion of CNC in anisole and cyclohexane has positive enthalpy; in the case of cyclohexane, thus suggests a lower interaction energy, as explained by (Parida et al. 2006). Some studies have focused on the wetting of hydrophobic powders (Hansford et al. 1980) or organomodified nanoclays (Dekany et al. 1986) by organic solvents, and it has been shown that positive immersion/wetting enthalpy suggests an entropy driven process (Hansford et al. 1980), while in the case of organomodified clays, endothermic swelling enthalpy is indicative of the process (Dekany et al. 1986). In our work, the aromatic surface graft we measured reduced the water/CNC surface interaction. However, a comparison of the immersion enthalpies of anisole and cyclohexane for grafted and neat CNC showed that although there was an absolute difference between the two molecules, in both cases CNC-g-BzAA displayed enthalpy that was approximately 0.5 J/g lower. In other words, no difference could be determined as a function of the chemical nature of the immersion liquid.

Table 2 Mixing temperaturess for CNC and CNC-g-BzAA with water, cyclohexane and anisole

Sample	Enthalpy of immersion (J g^{-1})		
	Water	Anisole	Cyclohexane
CNC	−0.23 ± 0.05	1.22 ± 0.12	1.78 ± 0.09
CNC-g-BzAA	1.14 ± 0.06	0.70 ± 0.13	1.29 ± 0.17

The contact angle values (Table 1) predicted better re-dispersion properties for grafted CNC. The aggregation of CNC in the dry state, due to hydrogen bonding between hydroxyls at the crystal surface, is a known problem that affects the storage and use of CNC in different fields, such as polymer additives. At present, CNC are generally shipped in an aqueous suspension that cannot readily be used in polymer

processes where dispersion of the CNC in either an organic solvent or a polymer melt is required. Figure 2 shows the re-dispersion of dried CNC and grafted CNC (with BzAA) in acetone after storage under ambient conditions. It can be seen that grafting greatly enhanced the dispersion of grafted CNC, while neat CNC remained aggregated and precipitated instantaneously.

Vapour/solid interactions between water or organic vapours and nanocellulose

Water sorption on surface grafted CNC

Figure 3a shows typical water sorption isotherms for the blank MCC and CNC samples, both of which displayed classic Type II sigmoidal sorption isotherms. Sorption behaviour may be related to surface area, crystallinity, porosity and the availability of hydroxyl groups on the surface. Both sorption isotherms are superposed in the low water activity range, a result that was also obtained by Belbekhouche et al. (2011) who worked on sisal CNC and MCC. According to Mihranyan et al. (2004), water sorption at low activities (<0.75) is determined by the crystallinity index of cellulose. The difference of approximately 10 % in the crystallinity index, and the difference in particle size (Table 1) apparently had no impact on sorption in the present case. However, at high water activities ($a_w > 0.6$), CNC took up much more water than MCC. This was not observed by Belbekhouche et al. 2011 who worked on MCC and CNC films, unlike our study in powders. The water adsorption of CNC increased by up to 170 % mass gain at $a_w = 0.9$, while the mass of MCC increased only by 12 %. The reason for this weight gain could be capillary condensation, a phenomenon already observed in some cases during the analysis of MCC powders (Mihranyan et al. 2004). Figure 3a also shows the water sorption on CNC-g-BzAA, where the supposed phenomenon of capillary condensation was suppressed. In order to obtain more details on this phenomenon, the volume of CNC granules and CNC-g-BzAA at different RH were monitored using environmental SEM. The resulting images are shown in Fig. 4, which clearly shows the swelling of CNC granules at 80 % RH (Fig. 4b) versus 40 % RH (Fig. 4a). Hysteresis of the sorption/desorption cycle is generally observed in porous structures. Figure 3a shows the hysteresis phenomenon in water sorption curves. The hysteresis curve for CNC-g-BzAA is representative of the shape seen for all grafted CNC. Percentage hysteresis is quantified in Fig. 3b. The hysteresis of CNC and MCC could be classified as type H3 (Sing 1985) which predicts the presence of plate-like structures, clearly describes the shape of cellulose whiskers and the occurrence of macropores inside aggregated nanocrystals (Fig. 4). Macropores allow the quite rapid desorption of condensed water. Some authors have suggested that MCC might also possess a degree of microporosity due to flaws in the microfibril structure (Kocherbitov et al. 2008). Water can penetrate by diffusion into even closed pores, but desorption would be much delayed. Under a vacuum, the "boiling" of MCC powders was observed, thus supporting this hypothesis (Kocherbitov et al. 2008). Kachrimanis et al. (2006) suggested that the hysteresis of water sorption isotherms at high water activities is caused by the creation of novel sorption sites inside de MCC structure, due to swelling of the amorphous phase. Mihranyan et al. (2004) found that hysteresis was higher in MCC with a lower crystallinity index, which supports the hypothesised influence of the amorphous phase. Here, a comparison of the data in Table 1 and Fig. 3b shows no correlation between the two quantities. Suppression of the water sorption hysteresis of grafted CNC was thus linked to the presence of the surface graft. Figures 4c, d show the

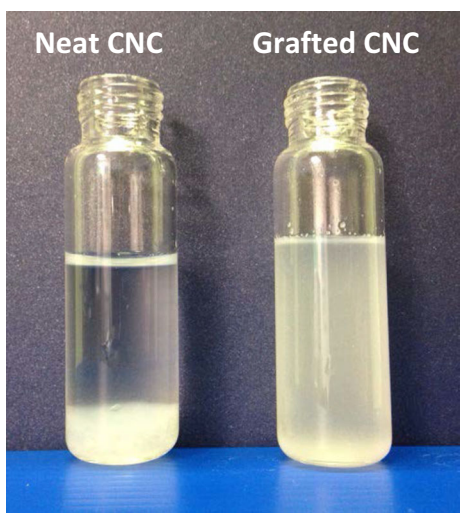

Fig. 2 Neat CNC and CNC-g-BzAA dispersed in acetone after drying

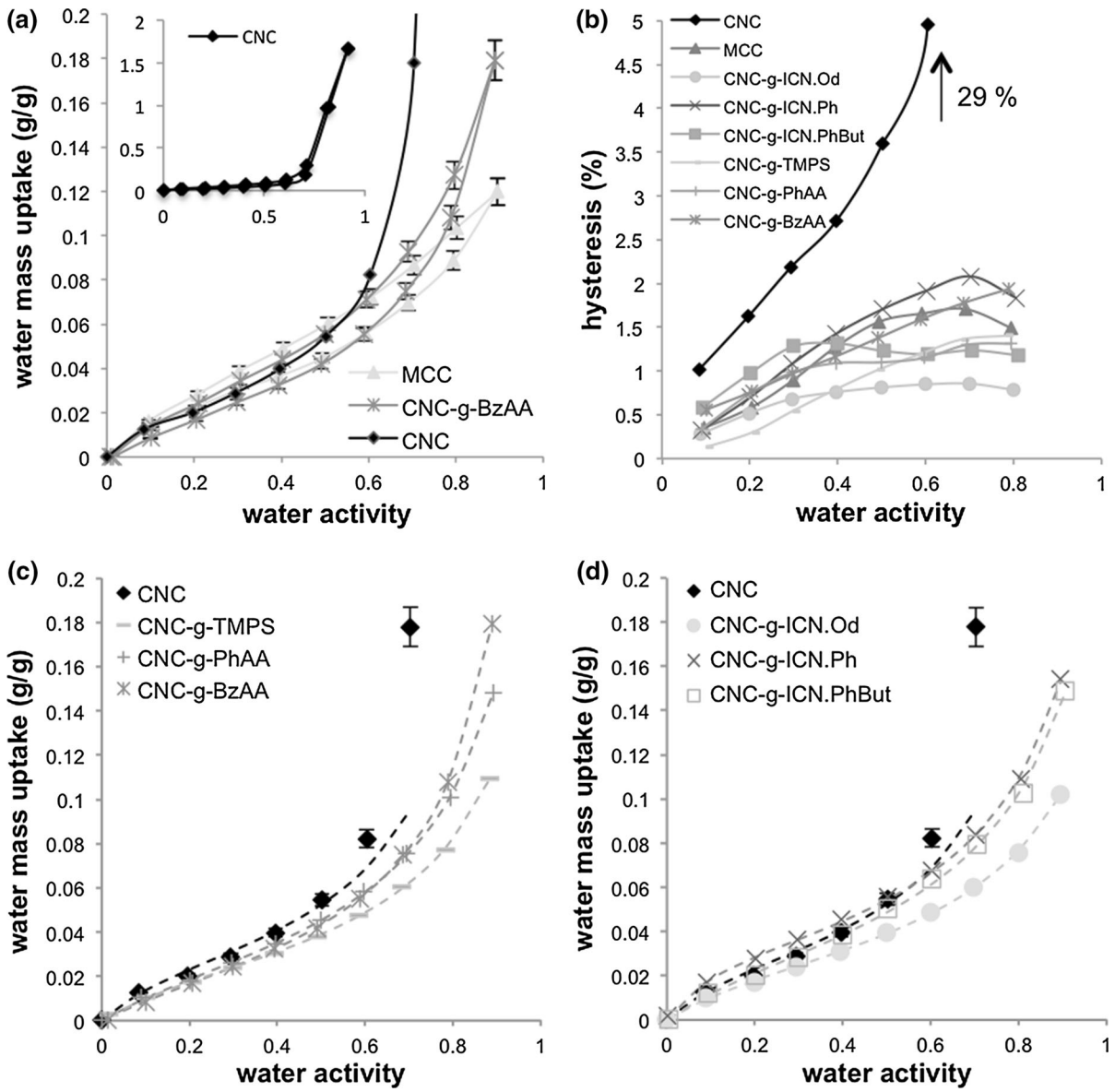

Fig. 3 Characteristics of the water sorption of microcrystalline cellulose (MCC), cellulose nanocrystals (CNC) and grafted CNC. **a** Water sorption of neat cellulose structures by comparison with grafted CNC, and the corresponding hysteresis loops. The *insert* shows the results regarding primary CNC on a different ordinate. **b** Percentage hysteresis of the whole sample set. Note that the hysteresis of CNC at water activity 0.7 is off the scale (29 %). **c**, **d** Water sorption isotherms of grafted CNC compared with neat CNC. *Dashed lines* show the sorption isotherm fit obtained using the GAB model

results of an environmental SEM analysis of CNC-g-BzAA powders at different RH. No changes in size were observed. The practical consequence of structural changes and hysteresis is the hornification of cellulose powders. The surface swelling of the powders due to water uptake can cause aggregation and closure of the pores in the granules. This causes problems in terms of storage and dispersion. The chemical surface modification was efficient in preventing capillary condensation in the cellulose structures, decreasing the hysteresis of sorption isotherms and decreasing of the granule swelling. These effects help protecting against hornification. Indeed, Fig. 2 shows the re-dispersability of grafted CNC in acetone.

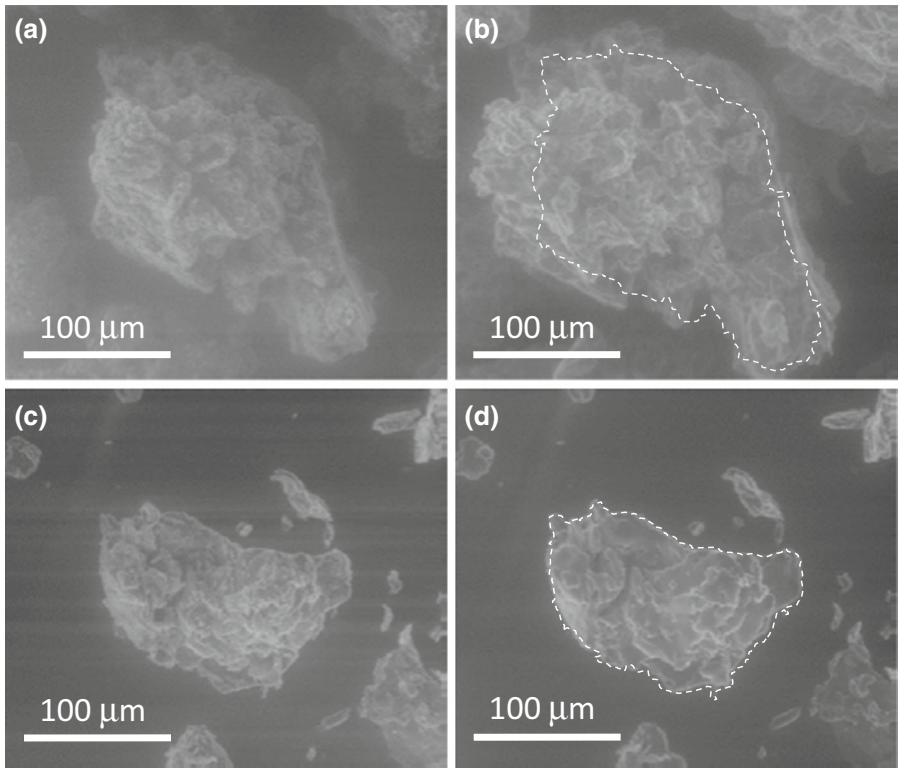

Fig. 4 Scanning electron microscopy (SEM) of CNC at **a** 20 °C, $a_w = 0.40$, 10 min. and **b** 9 °C, $a_w = 0.80$, 10 min.; of CNC-g-BzAA at **c** 20 °C, $a_w = 0.40$, 10 min. and **d** 9 °C, $a_w = 0.80$, 10 min. The *dashed white line* represents the contour of the granules at 40 % RH. This has been sketched to facilitate the comparison

Furthermore, grafted CNC lost its film-forming capacity after drying. GAB parameters relative to the heat of adsorption on the monolayer and upper layer, X_m, C and K, were calculated by fitting the GAB equation (Eq. 2) to the experimental sorption data relative to MCC and modified and unmodified CNC. These parameters are shown in Table 3, and the corresponding GAB isotherms in Fig. 3c, d (dashed lines). No differences were observed between the X_m values, except they were somewhat lower for CNC-g-ICN.Od and CNC-g-TMPS. Both grafts were apparently more effective in shielding the CNC from water penetration, probably because of high hydrophobicity (ICN.Od) and the creation of a condensed siloxane network (TMPS). It may seem surprising that the X_m of grafted CNC did not differ significantly from that of MCC, although macroscopic hydrophobicity, as measured by the contact angle and immersion studies, was very different. According to Young's theory, the contact angle is dependent on three interfacial tensions, where the fluid/solid contribution is also determined by interaction of the fluid with itself. The relationship between sorption and wettability is however not straightforward, and novel modelling work has revealed that the contact angle only plays a secondary role in determining the condensation pressure of water, while adsorption energy has a primary influence (Factorovich et al. 2014). The properties of water in the monolayer differ from those in the bulk, where the enthalpy of the sorbate is higher than that of the liquid. Molecules are absorbed locally in the monolayer without lateral interactions (Quirijns et al. 2005). Furthermore, the GAB model can predict incomplete surface coverage in the monolayer due to jamming of the molecules at the surface (Pradas et al. 2004). The C values for MCC and CNC were higher than those of the grafted CNC. This indicated a weaker interaction between the surface and water in the monolayer, because the surface grafts reduced the accessibility of hydroxyl groups.

The specific surface calculated from water sorption was higher than that obtained by N_2 sorption, thus

Table 3 GAB parameters of the sorption isotherms of water vapour, anisole and cyclohexane and specific surface areas for MCC and neat and grafted CNC

Sample	χ (%)	DS	Water vapour			S H_2O (m^2 g^{-1})	Anisole			S Anisole (m^2 g^{-1})	Cyclohexane			S Cyclohexane (m^2 g^{-1})
			X_m	C	K		X_m	C	K		X_m	C	K	
MCC	74	0	0.034	6.1	0.82	147	ND	ND	ND	ND	ND	ND	ND	ND
CNC	84	0	0.031	6.1	0.98	134	0.012	7.9	0.98	94	0.0073	2.4	0.79	68
CNC-g-ICN.Od	73	3	0.029	5.3	0.81	125	0.039	8.2	0.77	304	ND	ND	ND	ND
CNC-g-ICN.Ph	65	3	0.037	8.2	0.84	151	0.038	11.2	0.85	297	ND	ND	ND	ND
CNC-g-ICN.PhBut	69	2	0.036	4.6	0.85	156	0.028	12.4	0.93	219	ND	ND	ND	ND
CNC-g-TMPS	61	7	0.028	5.0	0.86	121	0.025	25.9	0.88	195	ND	ND	ND	ND
CNC-g-PhAA	77	5	0.034	3.9	0.88	147	0.067	5.7	0.74	523	0.025	3.7	0.79	233
CNC-g-BzAA	76	3	0.031	3.4	0.94	134	0.112	5.5	0.75	894	0.047	3.7	0.85	437

$R^2 > 0.997$ for all samples, * GAB model calculated for activities $a_w \leq 0.6$

For the sake of clarity the CNC crystallinity and substitution degrees are shown, repeating the data in Table 1

DS degree of substitution of 10 AGU moieties, *χ* crystallinity index, *S* specific surface area calculated from the different isotherms, X_m monolayer value of the GAB model, *C*, *K* GAB constants, *ND* not determined

demonstrating the ability of water to swell cellulose structures and penetrate the interstices of the sample (Portugal et al. 2010). The *K* values of the grafted CNC did not differ markedly from those of neat CNC, thus reflecting the observation that in the lower and middle ranges of water activity, the water sorption isotherms were only slightly affected.

Interaction of anisole and cyclohexane with CNC and grafted CNC

The idea behind this work was to develop CNC surface grafts that could suppress the hornification of CNC, facilitate its re-dispersibility *and* create specific interactions with volatile molecules containing aromatic functions. The impact of the chemical structure of the CNC surface graft on the anisole and cyclohexane sorption isotherm was therefore studied. Figure 5 plots the anisole and cyclohexane adsorption isotherms of unmodified and modified CNC. All isotherms were of type II and could be modelled using the GAB equation (Eq. 2). The model parameters are shown in Table 3. As expected, all grafted CNC took up more anisole than the blank sample. The lowest monolayer capacity was seen for CNC-g-TMPS. Interestingly, this sample also displayed the highest C value. Our interpretation is that the TMPS network offered a small accessible surface for anisole sorption and did not permit anisole penetration due to swelling. However, once anisole could sorb, a strong interaction between aromatic rings yielded an energetically very stable monolayer. Another interesting result concerned the comparison of different isocyanate grafts. The monolayer capacity of CNC-g-ICN.PhBut was lower than for the other two samples, even though it had the lowest grafting density (DS = 2; Table 1). Anisole was nevertheless strongly bound in the monolayer (high *C* value) and the system approached the properties of the bulk in the outer GAB layers (high *K* value). On the other hand, anisole seemed to be able to sorb in larger quantities in the aliphatic layer of CNC-g-ICN.Od, but the monolayer was less stable (lower C), while the GAB layers were relatively more structured (low *K* values). This hints at a positive impact of π–π interactions on sorption, which were clearly absent following sorption in the layer of the aliphatic graft. During a completely different experiment, Alia et al. (Alila et al. 2011) showed that it was possible to use starch nanocrystals modified by stearic acid to remove aromatic pollutants from water, but unfortunately they did not supply the DS in their paper. They cited the work of Thielemans et al. (2006), who measured a DS of approximately 2.6 (calculated from their data), and found a distance of approximately 0.75 nm between grafted aliphatic chains, which was sufficient to enable the diffusion of

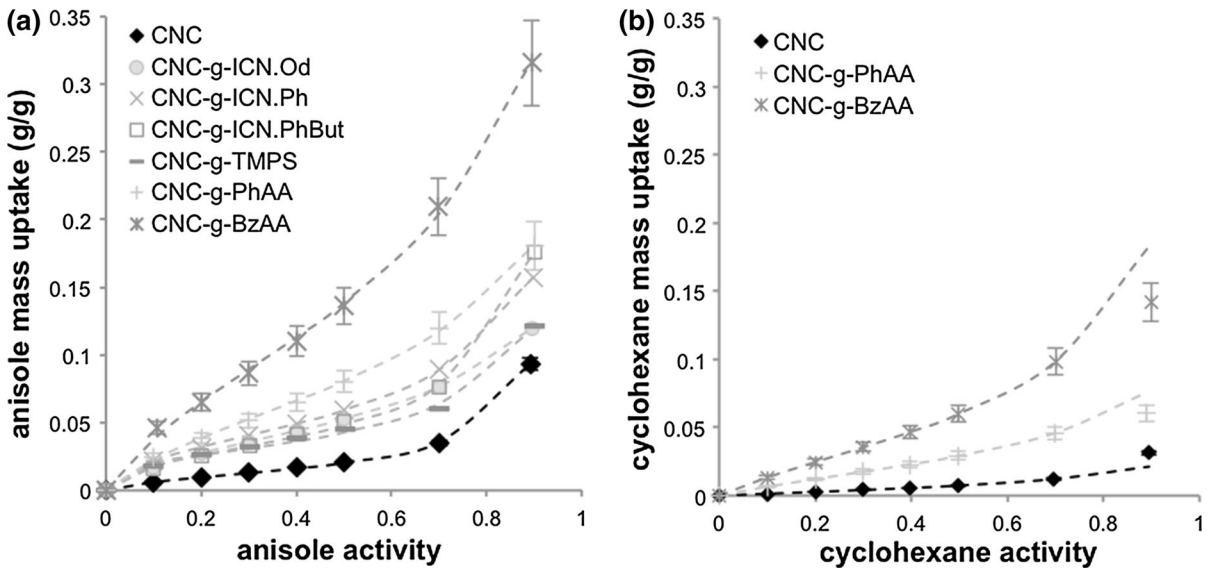

Fig. 5 Anisole (**a**) and cyclohexane (**b**) sorption isotherms for unmodified and modified CNC. *Dashed lines* show the sorption isotherm fit obtained using the GAB model. The experimental error was estimated at ±16 %

2-naphthol between stearate chains. The same mechanism may have accounted here for the high monolayer value of CNC-g-ICN.Od.

The comparison between aromatic molecules grafted with ester or urethane linkages also produced some interesting results. In the case of esterified molecules, the monolayer capacity almost doubled or tripled (Table 3), while the stability of anisole in the monolayer (*C* value) decreased. The *K* value was also low, which signified structured multilayers. It was apparent that these systems, and especially the more flexible CNC-g-BzAA system, permitted a higher uptake through swelling of the surface graft layers. The specific surface of CNC measured with anisole was smaller than that measured with water. In contrast, the S(anisole) of grafted CNC was higher then S(water). This result tended to confirm this swelling of the surface graft layer. However, it is necessary to achieve more accurate modelling of the surface properties or measurement of the fluorescence properties of the π-stacks in order to clarify the interpretation of this swollen surface structure. Confirmation of the importance of the aromatic structure to the sorption properties of the graft CNC was obtained from the sorption experiment with cyclohexane (Fig. 5b). This was performed on the CNC samples displaying the highest anisole uptake. A comparison of the isotherms of cyclohexane and anisole clearly showed the lower sorption of cyclohexane. The monolayer values and C constants of the cyclohexane isotherms were lower (Table 3), thus evidencing that fewer molecules were sorbed and GAB monolayers were less stabilized. The probed specific surface was consequently also lower than that of anisole, but higher compared to water. It was therefore possible to swell the surface graft layers with cyclohexane. Based on these data, we concluded that the grafting we describe offers an opportunity to selectively sorb aromatic molecules with CNC through the design of the surface graft. In the case of anisole, the creation of an ester linkage seems most favourable, and the structure of the surface graft needs to contain a flexible linker.

Figure 6 shows the hysteresis loops of the anisole and cyclohexane isotherms. Hysteresis could be classified as H4, indicating a mesoporous structure and swelling of the CNC (probably localized in the surface layer). The hysteresis loops of the anisole sorption isotherm were of greater amplitude than those of the cyclohexane sorption isotherm, which was compatible with the fact that less surface layer swelling was detected when cyclohexane was used as a probe. In both cases, hysteresis was negligible at low activities, which showed that the sorption was reversible and confirmed the possibility to create reusable absorbents.

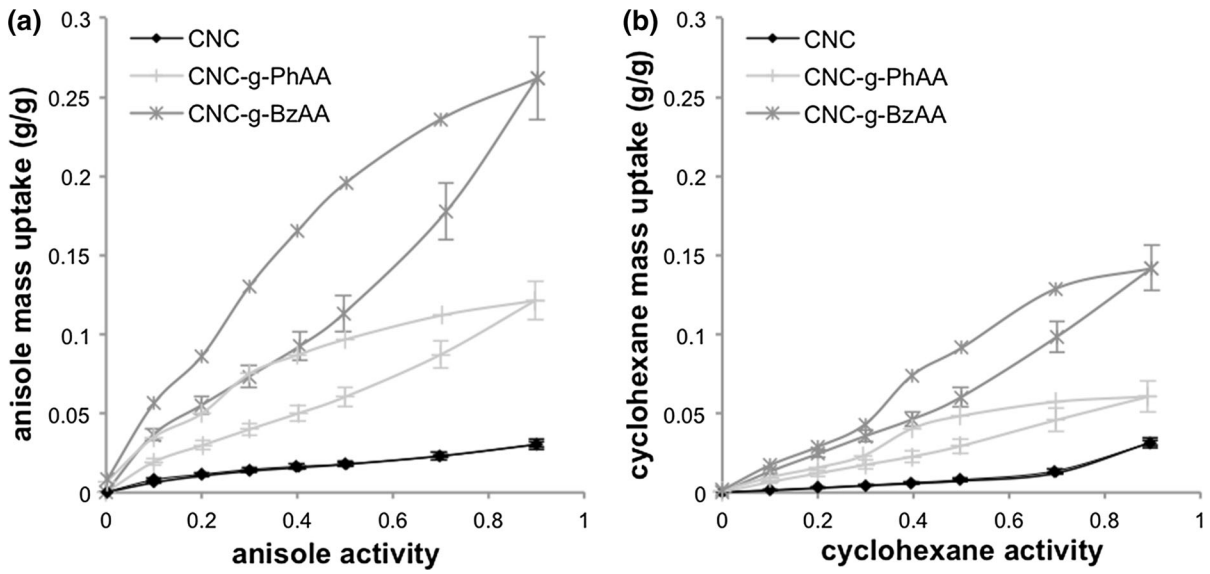

Fig. 6 Hysteresis loops of anisole (**a**) and cyclohexane (**b**) sorption isotherms for unmodified and modified CNC. *Dashed lines* show the sorption isotherm fit obtained using the GAB model

Conclusion

The aim of this work was to use CNC surface modifications in order to multiply the functionalities offered by CNC to host materials. The opportunities we identified regarding surface grafting were an increased compatibility with host polymers, reduced hornification, increased re-dispersability after drying, and an absorbent capacity for depollution or the controlled release of volatile molecules. An aromatic model system was chosen to obtain proof of concept because volatile molecules bearing aromatic functions have applicative importance in the aroma and fragrance industry. Furthermore, numerous environmental pollutants also bear aromatic moieties. It was shown that the use of aromatic surface grafts conferred a macroscopically hydrophobic, water-repellent character to CNC, while the water vapour sorption isotherms were only slightly affected. Hornification could be decreased and re-dispersability in organic solvents increased. The aromatic surface grafts were able to take up reversibly large quantities of the volatile aromatic compound anisole, where most probably swelling of the surface layer occurred. The non-aromatic compound cyclohexane was much less well sorbed. A comparison of different grafting techniques and surface graft structures showed that esterification of the CNC surface with carboxylic acids bearing a flexible linker chain afforded the highest sorption capacity.

In terms of perspectives, the grafted CNC powders will now be included in a polymer host matrix in order to probe the compatibility and study the impact of the CNC surface layer on polymer barrier properties.

Acknowledgments This work received support from the Mexican Scholarship Council (CONACyT) under Grant No. 213840. The authors wish to thank Monique Randrianarivo for her assistance with μ-DSC analysis.

References

Agrawal AM, Manek RV, Kolling WM, Neau SH (2004) Water distribution studies within microcrystalline cellulose and chitosan using differential scanning calorimetry and dynamic vapor sorption analysis. J Pharma Sci 93:1766–1779. doi:10.1002/jps.20085

Alila S, Boufi S (2009) Removal of organic pollutants from water by modified cellulose fibres. Ind Crops Prod 30:93–104. doi:10.1016/j.indcrop.2009.02.005

Alila S, Boufi S, Belgacem MN, Beneventi D (2005) Adsorption of a cationic surfactant onto cellulosic fibers—I. Surface charge effects. Langmuir 21:8106–8113. doi:10.1021/la050367n

Alila S, Aloulou F, Thielemans W, Boufi S (2011) Sorption potential of modified nanocrystals for the removal of aromatic organic pollutant from aqueous solution. Ind Crops Prod 33:350–357. doi:10.1016/j.indcrop.2010.11.010

Ambrosio-Martin J, Fabra MJ, Lopez-Rubio A, Lagaron JM (2015) Melt polycondensation to improve the dispersion of

bacterial cellulose into polylactide via melt compounding: enhanced barrier and mechanical properties. Cellulose 22:1201–1226. doi:10.1007/s10570-014-0523-9

Andrade RD, Lemus R, Perez CE (2011) Models of sorption isotherms for food: uses and limitations. Vitae 18:324–333

Belbekhouche S, Bras J, Siqueira G, Chappey C, Lebrun L, Khelifi B, Marais S, Dufresne A (2011) Water sorption behavior and gas barrier properties of cellulose whiskers and microfibrils films. Carbohydr Polym 83:1740–1748. doi:10.1016/j.carbpol.2010.10.036

Bondeson D, Mathew A, Oksman K (2006) Optimization of the isolation of nanocrystals from microcrystalline cellulose by acid hydrolysis. Cellulose 13:171–180. doi:10.1007/s10570-006-9061-4

Carpenter AW, de Lannoy CF, Wiesner MR (2015) Cellulose nanomaterials in water treatment technologies. Environ Sci Technol 49:5277–5287. doi:10.1021/es506351r

Clemenson S, Espuche E, David L, Leonard D (2010) Nanocomposite membranes of polyetherimide nanostructured with palladium particles: processing route, morphology and functional properties. J Membr Sci 361:167–175. doi:10.1016/j.memsci.2010.05.061

Dekany I, Szanto F, Nagy LG (1986) Sorption and immersional wetting on clay-minerals having modified surface. 2. Interlamellar sorption and wetting on organic montmorillonites. J Colloid Interface Sci 109:376–384. doi:10.1016/0021-9797(86)90316-4

Douillard J-M, Malandrini H (1999) Récents développements liés à l'enthalpie d'immersion. Comptes Rendus de l'Académie des Sciences - Series IIC - Chemistry 2:1–18. doi:10.1016/S1387-1609(99)80032-2

Dufresne A (2003) Interfacial phenomena in nanocomposites based on polysaccharide nanocrystals. Compos Interfaces 10:369–387. doi:10.1163/156855403771953641

Espino-Perez E, Bras J, Ducruet V, Guinault A, Dufresne A, Domenek S (2013) Influence of chemical surface modification of cellulose nanowhiskers on thermal, mechanical, and barrier properties of poly(lactide) based bionanocomposites. Eur Polym J 49:3144–3154. doi:10.1016/j.eurpolymj.2013.07.017

Espino-Perez E, Domenek S, Belgacem N, Sillard C, Bras J (2014) Green process for chemical functionalization of nanocellulose with carboxylic acids. Biomacromolecules 15:5441–5460. doi:10.1021/bm5013458

Espino-Perez E, Gilbert RG, Domenek S, Brochier-Salon MC, Belgacem MN, Bras J (2016a) Nanocomposites with functionalised polysaccharide nanocrystals through aqueous free radical polymerisation promoted by ozonolysis. Carbohydr Polym 135:256–266. doi:10.1016/j.carbpol.2015.09.005

Espino-Perez E, Domenek S, Brochier Salon M-C, Belgacem N, Bras J (2016b) Study of cellulose nanocrystals grafted alkoxysilane: hydrolysis–condensation effects. Personal communication (publication to be submitted)

Eyley S, Thielemans W (2014) Surface modification of cellulose nanocrystals. Nanoscale 6:7764–7779. doi:10.1039/c4nr01756k

Factorovich MH, Solveyra EG, Molinero V, Scherlis DA (2014) Sorption isotherms of water in nanopores: relationship between hydropohobicity, adsorption pressure, and hysteresis. J Phys Chem C 118:16290–16300. doi:10.1021/jp5000396

Fang X, Vitrac O, Domenek S, Ducruet V (2012) Controlling the molecular interactions to improve the diffusion barrier of biosourced polymers to organic solutes. Defect Diffus Forum 323–325:269–274. doi:10.4028/www.scientific.net/DDF.323-325.269

Follain N, Belbekhouche S, Bras J, Siqueira G, Marais S, Dufresne A (2013) Water transport properties of bionanocomposites reinforced by *Luffa cylindrica* cellulose nanocrystals. J Membr Sci 427:218–229. doi:10.1016/j.memsci.2012.09.048

Fortunati E, Peltzer M, Armentano I, Jimenez A, Kenny JM (2013) Combined effects of cellulose nanocrystals and silver nanoparticles on the barrier and migration properties of PLA nano-biocomposites. J Food Eng 118:117–124. doi:10.1016/j.jfoodeng.2013.03.025

Habibi Y (2014) Key advances in the chemical modification of nanocelluloses. Chem Soc Rev 43:1519–1542. doi:10.1039/c3cs60204d

Habibi Y, Lucia LA, Rojas OJ (2010) Cellulose nanocrystals: chemistry, self-assembly, and applications. Chem Rev 110:3479–3500. doi:10.1021/cr900339w

Hansford DT, Grant DJW, Newton JM (1980) Surface energetics of the wetting of a hydrophobic powder. J Chem Soc Faraday Trans I 76:2417–2431. doi:10.1039/f19807602417

Hanson B, Pryamitsyn V, Ganesan V (2012) Computer simulations of gas diffusion in polystyrene-C-60 fullerene nanocomposites using trajectory extending kinetic Monte Carlo method. J Phys Chem B 116:95–103. doi:10.1021/jp209294t

Kachrimanis K, Noisternig MF, Griesser UJ, Malamataris S (2006) Dynamic moisture sorption and desorption of standard and silicified microcrystalline cellulose. Eur J Pharm Biopharm 64:307–315. doi:10.1016/j.ejpb.2006.05.019

Kocherbitov V, Ulvenlund S, Kober M, Jarring K, Arnebrant T (2008) Hydration of microcrystalline cellulose and milled cellulose studied by sorption calorimetry. J Phys Chem B 112:3728–3734. doi:10.1021/jp711554c

Korhonen JT, Kettunen M, Ras RHA, Ikkala O (2011) Hydrophobic nanocellulose aerogels as floating, sustainable, reusable, and recyclable oil absorbents. ACS Appl Mater Interfaces 3:1813–1816. doi:10.1021/am200475b

Lam E, Male KB, Chong JH, Leung ACW, Luong JHT (2012) Applications of functionalized and nanoparticle-modified nanocrystalline cellulose. Trends Biotechnol 30:283–290. doi:10.1016/j.tibtech.2012.02.001

Lemahieu L, Bras J, Tiquet P, Augier S, Dufresne A (2011) Extrusion of nanocellulose-reinforced nanocomposites using the dispersed nano-objects protective encapsulation (DOPE). Process Macromol Mater Eng 296:984–991. doi:10.1002/mame.201100015

Lu P, Hsieh Y-L (2010) Preparation and properties of cellulose nanocrystals: rods, spheres, and network. Carbohydr Polym 82:329–336. doi:10.1016/j.carbpol.2010.04.073

Lu P, Hsieh Y-L (2012) Preparation and characterization of cellulose nanocrystals from rice straw. Carbohydr Polym 87:564–573. doi:10.1016/j.carbpol.2011.08.022

Mariano M, El Kissi N, Dufresne A (2014) Cellulose nanocrystals and related nanocomposites: review of some properties and challenges. J Polym Sci B Polym Phys 52:791–806. doi:10.1002/polb.23490

Mihranyan A, Llagostera AP, Karmhag R, Strømme M, Ek R (2004) Moisture sorption by cellulose powders of varying crystallinity. Int J Pharm 269:433–442. doi:10.1016/j.ijpharm.2003.09.030

Morandi G, Heath L, Thielemans W (2009) Cellulose nanocrystals grafted with polystyrene chains through surface-initiated atom transfer radical polymerization (SI-ATRP). Langmuir 25:8280–8286. doi:10.1021/la900452a

Parida SK, Dash S, Patel S, Mishra BK (2006) Adsorption of organic molecules on silica surface. Adv Colloid Interface 121:77–110. doi:10.1016/j.cis.2006.05.028

Park S, Baker J, Himmel M, Parilla P, Johnson D (2010) Cellulose crystallinity index: measurement techniques and their impact on interpreting cellulase performance. Biotechnol Biofuels 3:1–10. doi:10.1186/1754-6834-3-10

Portugal I, Dias VM, Duarte RF, Evtuguin DV (2010) Hydration of cellulose/silica hybrids assessed by sorption isotherms. J Phys Chem B 114:4047–4055. doi:10.1021/jp911270y

Pradas MM, Sanchez MS, Ferrer GG, Ribelles JLG (2004) Thermodynamics and statistical mechanics of multilayer adsorption. J Chem Phys 121:8524–8531. doi:10.1063/1.1802271

Quirijns EJ, van Boxtel AJB, van Loon WKP, van Straten G (2005) Sorption isotherms, GAB parameters and isosteric heat of sorption. J Sci Food Agric 85:1805–1814. doi:10.1002/jsfa.2140

Rodrigues FHA, Spagnol C, Pereira AGB, Martins AF, Fajardo AR, Rubira AF, Muniz EC (2014) Superabsorbent hydrogel composites with a focus on hydrogels containing nanofibers or nanowhiskers of cellulose and chitin. J Appl Polym Sci 131:39725. doi: 10.1002/app.39725

Roskar R, Kmetec V (2005) Evaluation of the moisture sorption behaviour of several excipients by BET, GAB and microcalorimetric approaches. Chem Pharm Bull 53:662–665. doi:10.1248/cpb.53.662

Salazar R, Domenek S, Ducruet V (2014) Interactions of flavoured oil in-water emulsions with polylactide. Food Chem 148:138–146

Sèbe G, Ham-Pichavant F, Ibarboure E, Koffi ALC, Tingaut P (2012) Supramolecular structure characterization of cellulose II nanowhiskers produced by acid hydrolysis of cellulose I substrates. Biomacromolecules 13:570–578. doi:10.1021/bm201777j

Sing KSW (1985) Reporting physisorption data for gas/solid systems with special reference to the determination of surface area and porosity. (Recommendations 1984). Pure Appl Chem 57:603–619. doi:10.1351/pac198557040603

Siqueira G, Bras J, Dufresne A (2010) New process of chemical grafting of cellulose nanoparticles with a long chain isocyanate. Langmuir 26:402–411. doi:10.1021/la9028595

Thielemans W, Belgacem MN, Dufresne A (2006) Starch nanocrystals with large chain surface modifications. Langmuir 22:4804–4810. doi:10.1021/la053394m

Timmermann EO (2003) Multilayer sorption parameters: BET or GAB values? Colloid Surf A Physicochem Eng Asp 220:235–260. doi:10.1016/s0927-7757(03)00059-1

Van Den Berg C (1984) Description of water activity of food for engineering purposes by means of the GAB model of sorption. Eng Foods 1:311–320

Volkova N, Ibrahim V, Hatti-Kaul R, Wadso L (2012) Water sorption isotherms of Kraft lignin and its composites. Carbohydr Polym 87:1817–1821. doi:10.1016/j.carbpol.2011.10.001

Wu WB, Zhang L (2014) Functionalization and applications of nanocrystalline cellulose. Prog Chem 26:403–414. doi:10.7536/pc130657